Materials Science & Engineering C 118 (2021) 111419

Contents lists available at ScienceDirect

Materials Science & Engineering C

journal homepage: www.elsevier.com/locate/msec

Air-jet spinning corn zein protein nanofibers for drug delivery: Effect of biomaterial structure and shape on release properties

Kelsey DeFrates[a,b,1], Theodore Markiewicz[b,1], Ye Xue[a,b], Kayla Callaway[a], Christopher Gough[b,c], Robert Moore[a], Kristen Bessette[b], Xiaoyang Mou[c], Xiao Hu[a,b,d,*]

[a] Department of Physics and Astronomy, Rowan University, Glassboro, NJ 08028, USA
[b] Department of Biomedical Engineering, Rowan University, Glassboro, NJ 08028, USA
[c] Department of Chemistry and Biochemistry, Rowan University, Glassboro, NJ 08028, USA
[d] Department of Molecular and Cellular Biosciences, Rowan University, Glassboro, NJ 08028, USA

ARTICLE INFO

Keywords:
Corn zein protein
Air-jet spinning
Drug release
Nanofiber
Film
Secondary structure

ABSTRACT

Nanofiber materials are commonly used as delivery vehicles for dermatological drugs due to their high surface-area-to-volume ratio, porosity, flexibility, and reproducibility. In this study air-jet spinning was used as a novel and economic method to fabricate corn zein nanofiber meshes with model drugs of varying solubility, molecular weight and charge. The release profiles of these drugs were compared to their release from corn zein films to elucidate the effect of geometry and structure on drug delivery kinetics. In film samples, over 50% of drug was released after only 2 h. However, fiber samples exhibited more sustained release, releasing less than 50% after one day. FTIR, SEM, and DSC were performed on nanofibers and films before and after release of the drugs. Structural analysis revealed that the incorporation of model drugs into the fibers would transform the zein proteins from a random coil network to a more alpha helical structure. Upon release, the protein fiber reverted to its original random coil network. In addition, thermal analysis indicated that fibers can protect the drug molecules in high temperature above 160 °C, while drugs within films will degrade below 130 °C. These findings can likely be attributed to the mechanical infiltration of the drug molecules into the ordered structure of the zein fibers during their solution fabrication. The slow release from fiber samples can be attributed to this biophysical interaction, illustrating that release is dictated by more than diffusion in protein-based carriers. The controlled release of a wide variety of drugs from the air-jet spun corn zein nanofiber meshes demonstrates their success as drug delivery vehicles that can potentially be incorporated into different biological materials in the future.

1. Introduction

Topical delivery of dermatological drugs offers many advantages over systemic delivery routes such as the requirement for lower doses and reduced off-target effects [1,2]. The development of drug delivery vehicles in various dimensions such as micelles [3,4], liposomes [5,6], nanoparticles [3,5,7], and thin films [8,9], has allowed for long-term, controlled release of topical drugs when these systems are placed on the skin, increasing patient compliance and efficacy of the treatment. Most notably, polymeric nanofibers exhibit unique qualities that make them ideal candidates for topical drug delivery. For example, the high surface area-to-volume ratios of nanofibers allows for efficient delivery of hydrophobic and hydrophilic drugs that can be easily incorporated into the pre-fiber solution [2,7,10]. Malleable fiber mats also exhibit high porosity essential in mass transport and can be easily incorporated into bandages for the treatment of wounds [2,7]. However, clinical use of nanofiber mats in topical drug delivery has been limited most likely due to a lack of quantitative research and problems with controllable, industrial-scale production [7].

To date, the most common fabrication method for protein nanofibers is electrospinning [11,12]. In this approach, a polymer solution is expelled from a spinneret connected to a high voltage source above a grounded collector. At the outlet of a spinneret, the liquid becomes charged and is drawn towards the direction of the collector, as electrostatic repulsions overpower surface tension forces. Simple improvements to the electrospinning apparatus, can also be used to create multi-component fibers, exhibiting a core-shell or Janus-like structure [13–16]. However, in all of these techniques, a high voltage power

* Corresponding author.
E-mail address: hu@rowan.edu (X. Hu).
[1] Contributed equally to this manuscript.

https://doi.org/10.1016/j.msec.2020.111419
Received 11 March 2020; Received in revised form 11 August 2020; Accepted 18 August 2020
Available online 22 August 2020
0928-4931/

source is required to facilitate fiber formation [17]. To eliminate this need and improve the efficiency of fiber formation while maintaining cost effectiveness, an air-jet spinning technique was developed to create protein-based fibers. Air-jet spinning, also referred to as solution blowing, utilizes compressed air as the main driving force for fiber formation [19,20]. The apparatus involves inserting polymer solution into one side of a concentric nozzle spray gun, attached to an air compressor. High-speed gas is then passed through the gun, applying a shear force to the polymer solution to create strands. As these polymer strands enter the atmosphere, the solvent quickly evaporates, resulting in the formation of fibrous mats [18,19].

In this study, the air-jet spinning method was used to fabricate corn zein protein nanofibers for controlled release of various model drugs, chosen to reflect the diversity of pharmaceutical compounds used today. Zein, the major storage protein in corn, exhibits extremely high tensile strength, flexibility, and toughness, making it an ideal polymer for air-jet spinning and fiber formation [21]. Recently, Wang et al. formulated corn zein nanoribbons through a modified coaxial electrospinning process, yielding uniform structures with tunable diameters [22]. As a drug delivery vehicle, the proposed anti-bacterial, anti-microbial, and antioxidative properties of corn zein make it a promising candidate for topical delivery [23,24]. By fabricating bilayer membranes composed of zein films and electrospun fibers, Kimna et al. created mechanically robust wound dressings, with structural similarities to native skin [25]. Electrospun corn zein fibers have also been loaded with antimicrobial compounds such as tetracycline hydrochloride, as well as poorly soluble drugs such as indomethacin [26,27–31].

Due to the variety of drug delivery vehicles available today, the effect of carrier geometry on drug loading, storage, and release kinetics has garnered much interest in the field of drug delivery [32–34]. Understanding this relationship will ultimately lead to more precise tuning and design of drug delivery systems. To explore this concept, model drug release from cylindrical zein nanofibers was also compared to surface release from zein films, synthesized through the solvent casting method. All fibers and films were also characterized with FTIR, SEM, and DSC and differences in drug loading and corn zein structure were noted.

2. Experimental section

2.1. Materials preparation

Purified zein protein powder (CAS Number 9010-66-6) was a gift obtained from POET, LLC (Sioux Falls, SD, USA) and filtered through a 0.45 μm nylon membrane to remove excess impurities once dissolved. ACS Grade 98% Formic Acid was purchased from EMD Millipore Corporation (Burlington, MA, USA), ACS Grade Calcium Chloride Anhydrous was purchased from AMRESCO Inc. (Solon, OH, USA), and both were used as purchased. Crystal violet, indigo carmine, alcian blue 8GX, rhodamine B, and rifampin were purchased from VWR International (Bridgeport, NJ, USA).

2.2. Corn zein nanofibers

Fabrication of corn zein nanofibers (Fig. 1 and Supplemental Fig. 1) began by dissolving approximately 16 g of corn zein protein in 30 mL of formic acid (pH = 2.3) at room temperature. This concentration was chosen based on preliminary experiments exploring the effect of zein concentration on fiber formation. Below this concentration, fibers were unable to support their own weight and collapsed during collection, due to their low protein content. At higher concentrations, however, the solution became too viscous for the spray gun, and fiber formation was not achieved. While corn zein is soluble in many organic compounds including ethanol/water solutions, it exhibits higher dissolution in mild organic acids, such as formic and acetic acid mainly due to increased protonation [35]. High concentration zein-formic acid solutions also exhibit lower viscosities compared to corresponding ethanol mixtures, preventing clogging of the spray gun.

For samples containing model drugs, 0.4 g of drugs were dissolved in the formic acid prior to the addition of corn zein. After successful dissolution of zein protein, the solution was filtered through a syringe to remove any impurities and residual zein. The final filtered solution was then transferred to a syringe which was attached to a NEO BCN Siphon-Feed Dual-Action Airbrush from Anest Iwata-Medea, Inc. (Portland, OR, USA). Compressed air, generated by a DeWalt D55168 air compressor (Baltimore, MD, USA), was fed into the spray gun at a pressure of 100 psi and used to shear the zein solution to produce fibers. Fibers were collected on a box lined with aluminum foil that was approximately 1.7 m away from the sprayer and left to dry. Excess formic acid was evaporated by placing the fibers into a vacuum oven at 60 °C for 12 h. Absence of the C═O peak is observed in FTIR of all fiber samples, further suggesting that there was no residual formic acid left before the studies. Finally, fibers were characterized, and used for drug release studies.

A summary of chemical and physical properties of the chosen model drugs is shown in Table 1. A low concentration of drug was used to prevent clogging of the spray gun nozzle by model drug crystals. As seen in Table 1, the model drugs that were chosen to represent varying hydrophobicity, molecular weights, and solubilities, reflecting the library of pharmaceutical compounds used today.

2.3. Corn zein films

To study the effect of morphology on drug release kinetics, corn zein films were also fabricated and compared to fibers (Fig. 1). Same corn zein-drug formic acid solutions were made as described above. Approximately 3 mL of the solution was then poured into circular PDMS molds and left to sit at room temperature for two days. To remove excess formic acid, films were also placed in the vacuum oven at 60 °C for 12 h. Films containing each model drug were used for characterizations, as well as drug release studies.

2.4. SEM characterization

Scanning Electron Microscopy (SEM) was used to assess morphological characterization of the zein fibers and films. The experiments were performed using a Leo 1530 VP SEM (Germany), all the samples were sputtered coated with gold for SEM imaging for 9 s. All figures were obtained with EHT at 5.00 kV.

2.5. Fourier transform infrared spectrometry (FTIR)

A Bruker Tensor 27 Fourier Transform Infrared Spectrometer (Billerica, MA, USA), equipped with a deuterated triglycine sulfate detector and a multiple reflection, horizontal MIRacle ATR attachment (using a Ge crystal, from Pike Tech. (Madison, WI)) that was continuously purged with nitrogen gas was used. Readings were taken at a range of 4000 to 400 cm^{-1} with 64 background scans and 64 sample scans at a of 4 cm^{-1}. For each fiber and film sample, four total measurements were taken to ensure homogeneity. However, only one spectrum is shown in this report to demonstrate the overall trend. Between samples, the ATR crystal was cleaned with methanol.

2.6. Differential scanning calorimetry (DSC)

Data were collected using a TA Instruments (New Castle, DE, USA) Q100 DSC, with purged dry nitrogen gas flow (50 mL/min), equipped with a refrigerated cooling system. The instrument had been previously calibrated with indium for heat flow and temperature, and aluminum and sapphire reference standards were used to calibrate heat capacity. Samples were encapsulated in aluminum pans and heated in the DSC.

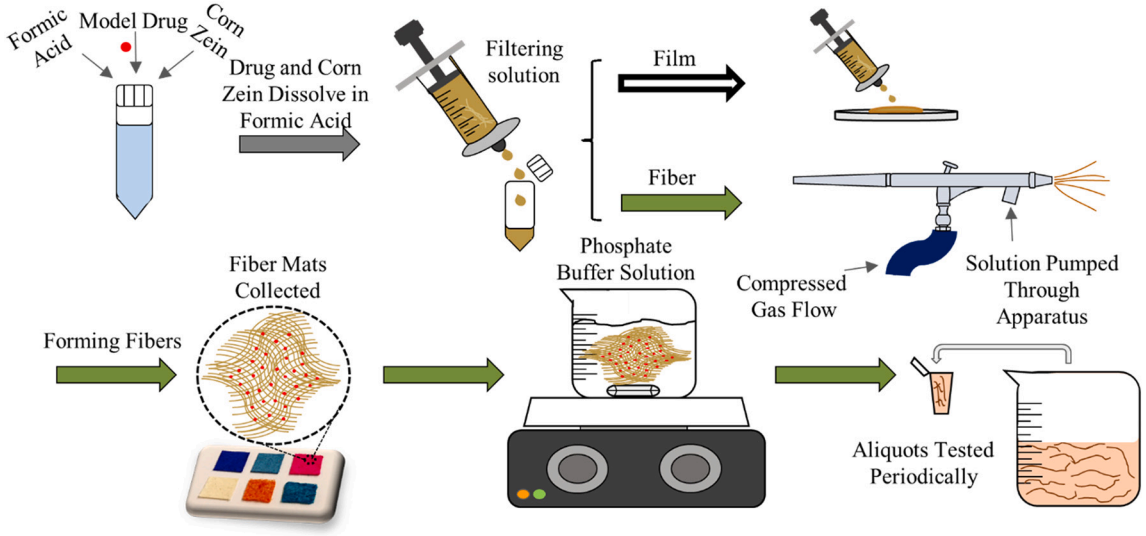

Fig. 1. Overview of corn zein nanofiber and films synthesis and drug release study procedure.

Temperature-modulated differential scanning calorimetry (TMDSC) measurements were taken at a heating rate of 2 °C/min with a modulation period of 60s and temperature amplitude of 0.318 °C, from −40 °C to 400 °C.

2.7. Drug release study

Drug release experiments were performed in continuous sink conditions, by first immersing 0.05 g of drug-loaded film or fiber meshes, into 50 mL of 20 mM phosphate buffer (pH 7.0) at 37 °C. At

Table 1
Summary of chemical and physical properties of the chosen model drugs.

Model drug compound	Molecular weight (g/mol)	Solubility in H_2O at 25 °C (mg/mL)	Log P
Crystal violet 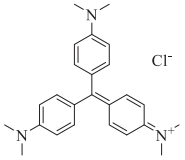	407.98	50	1.4
Indigo carmine 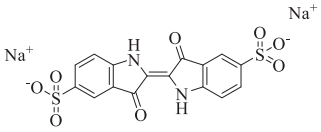	466.36	10	1.01
Rhodamine B 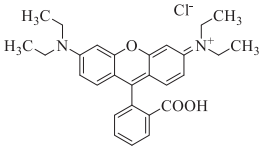	497.02	8	1.95
Rifampin 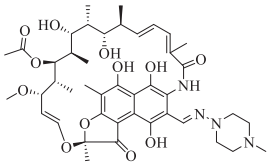	822.94	2.5	2.77
Alcian blue 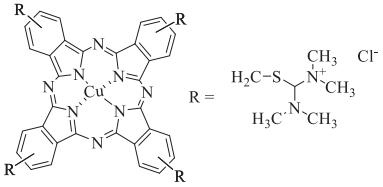	1298.9	1	−9.7

predetermined time points (15 min, 30 min, 1 h, 2 h, 3 h, 4 h, 5 h, 24 h, 48 h, 96 h), samples were transferred to fresh PBS and 2 mL aliquots of the previous bath were collected for analysis. To quantify the concentration of drug in the release media, the UV absorbance of the aliquots was measured using a SpectraMax i3x Plate Reader (Molecular Devices LLC, Sunnyvale, CA, USA) immediately after collection. Absorbance was correlated to concentration using a standard prepared by dissolving the corresponding drug in PBS at various concentrations. All experiments were done in triplicate, and the average values graphed as a function of time. Upon completion of the study, fibers were extracted from solution via suction filtration and dried overnight. Release profiles were then fit with the Krosmeyer-Peppas release model shown in Eq. (1) [36]:

$$\frac{M_t}{M_\infty} = K_{kp} t^n \quad (1)$$

Here, M_∞ represented the amount of drug released at the equilibrium (assumed to be the total amount of drug loaded) and M_t corresponds to drug released at specific time point. The fitted constant K, accounts for the physiochemical and geometric characteristics of the carrier, and n corresponds to the mechanism of release.

2.8. Biocompatibility study

HEK293 (Human embryonic kidney) cells from ATCC (American Type Culture Collection) were grown in Dulbecco's modified Eagle's medium (HyClone, with 4.00 mM L-Glutamine and 4500 mg/L Glucose), supplemented with 10% fetal bovine serum (Life Technologies Inc.) and 100 U/mL Penicillin-Streptomycin (Thermo Fisher Scientific Inc., USA), in an atmosphere of 95% air, 5% carbon dioxide (CO_2), at 37 °C. Cell culture was carried out according to NIH standard protocols. Equal number of cells was seeded on different zein fiber mat or film samples at a concentration of 3×10^4 cells per well with blank substrates as the control samples. All samples prepared in triplicate on the same 96 well plate (Costar, Corning Life Sciences, Corning, NY, USA). Cell numbers were acquired 72 h after seeding using a 3-[4,5-dimethylthiazole-2-yl]-2,5-diphenyltetrazolium bromide (MTT) assay following protocols from the manufacturer. 100 uL of MTT solution was added to each well and incubated at 37 °C with 150uL of dimethylsulfoxide (DMSO). After homogenizing the solution via 30 min of shaking, absorbance measurements were taken using a plate reader.

3. Results and discussion

3.1. Structural characterization

To assess the structural properties of the corn zein nanofibers, samples with and without model drugs were first characterized with FTIR. Fig. 2a shows the complete absorbance spectrum of samples before drug release. Absence of the formic acid C=O peak is also observed in FTIR of all film samples, suggesting that no residual formic acid was left before the studies. To analyze the secondary structure of the corn zein protein more closely, the Amide *I* and II regions are highlighted in Fig. 2b. Prior to the addition of model drugs, the Amide *I* peak is localized at 1640 cm^{-1} suggesting an insoluble network dominated by random coils. Upon addition of model drugs, the Amide *I* peak shifts left suggesting a transition to a more alpha helical structure. For the crystal violet and rhodamine B samples, a shoulder at 1585 cm^{-1} and 1560 cm^{-1} can be seen. These peaks can be attributed to the corresponding model drugs (Supplemental Fig. 2). All samples excluding fibers containing no drug or crystal violet also exhibit a small shoulder localized at 1720 cm^{-1}, most likely originating from the C=O stretching of the protein due to the structural change [37,38]. These assertions are further corroborated by the spectrum shown in Fig. 2c for fibers after drug release. A shift back to the original 1640 cm^{-1} localization of the Amide *I* region is observed for all fiber samples once the drug is removed. This suggests that the model drug molecules may be pushing the random coil structure of the corn zein into alpha helices. Upon removal of the drug, corn zein again completely adopts it native

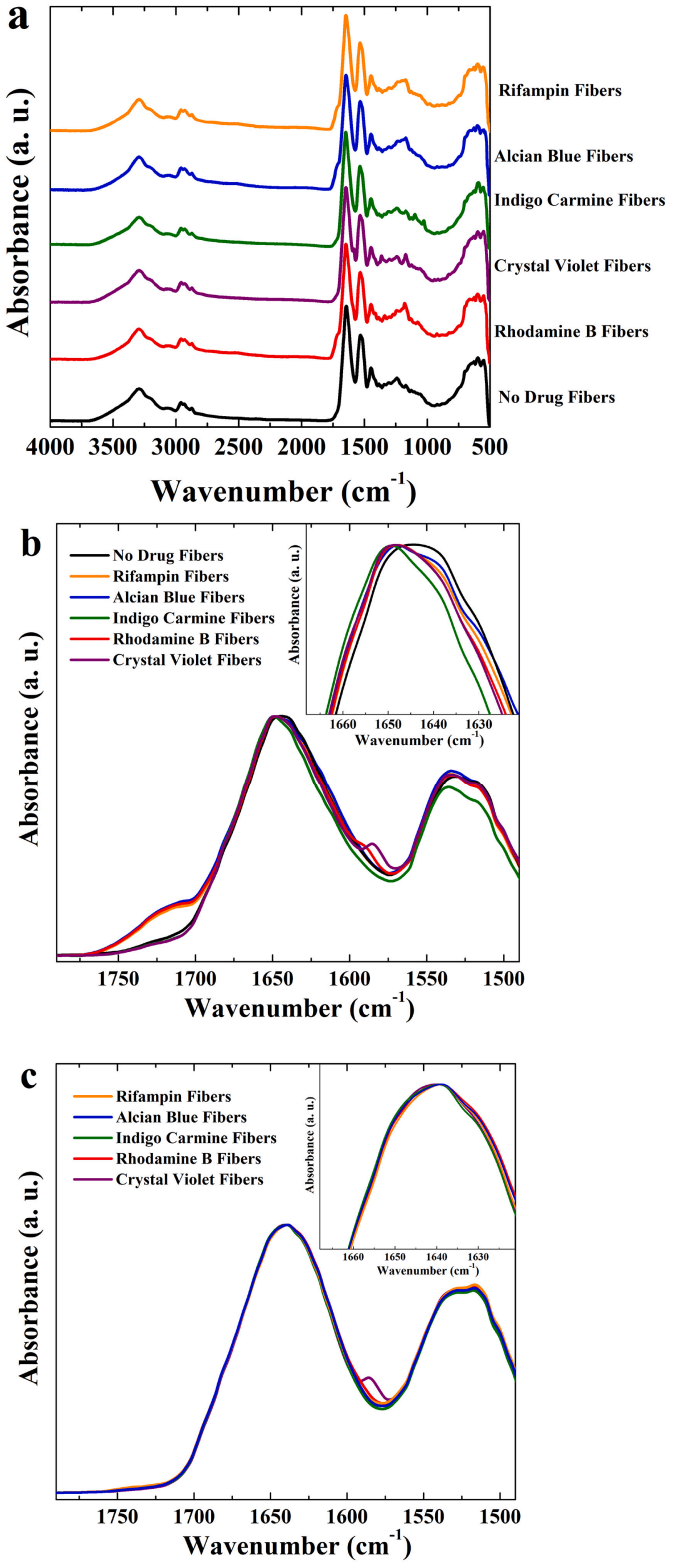

Fig. 2. (A) FTIR spectra for corn zein nanofibers with and without different model drugs. The region containing the amide I and II peaks has been isolated in (B) to highlight the random coil to alpha helix transition with the addition of drug. When drug is released, secondary structure reverts back to homogeneous random coil network in (C).

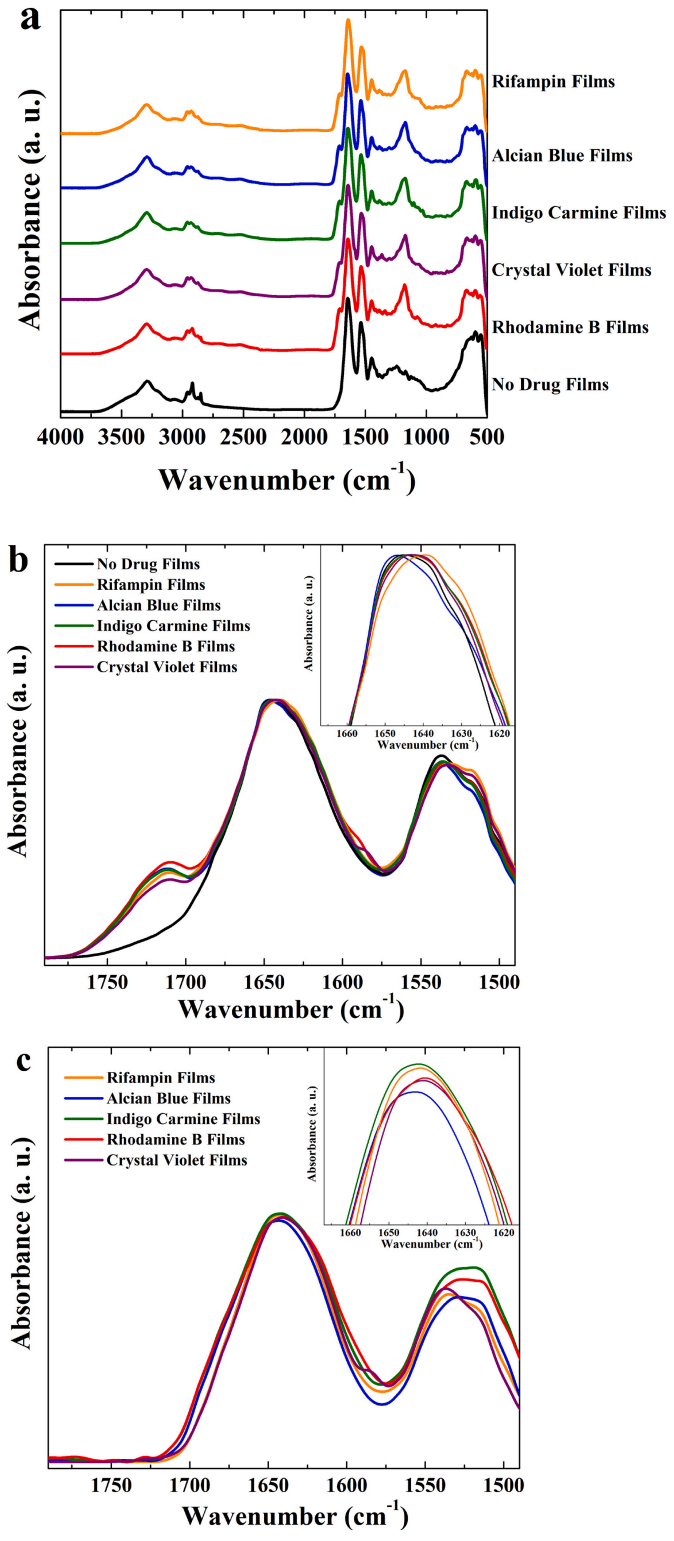

Fig. 3. (A) FTIR spectra of corn zein films with and without model drugs. The region containing the amide I and II peaks has been isolated in (B) to show the effects of drug incorporation on zein structure. After release, films maintain their inhomogeneous coil network with some variety as seen in (C).

coil-dominated structure, illustrating a fully controllable transition overall. Reduction in the rhodamine B and crystal violet peaks is also evident, suggesting that the majority of the drug was released. In this instance, the corn zein fibers are behaving more like carriers for the model drugs. This is an ideal characteristic for drug delivery vehicles since the drug does not permanently bind to the protein and can be released completely.

Fig. 3a and b show the complete and Amide *I* and II spectrum of the corn zein films prior to drug release. Compared to the fiber samples studied in Fig. 1b, the corn zein films appeared to retain their random coil structure upon the addition of model drugs. During the creation of films, corn zein is dissolved in formic acid and then poured into PDMS molds to set. In this instance, the corn zein is exposed to formic acid for a longer period of time than it is during fiber generation. During this time, the formic acid is able to sever some of the hydrogen bonds of the corn zein structure, allowing the integration of the model drug molecules. Thus, the addition of drugs does not compress the corn zein towards a more alpha helical structure for the films. An exception to this is films containing alcian blue and rifampin. As seen in Fig. 3b, alcian blue films experienced a similar shift to 1648 cm^{-1}. Alcian blue, with a molecular weight of 1.3 kDa was the largest model drug tested. This drug is most likely too large to integrate into the corn zein structure and still pushes the protein towards an alpha helical structure. Upon release of drug from the films, the majority of the random coil network is maintained but with slight structural change, illustrating an uncontrollable transition due to the protein-drug interactions.

3.2. Thermal analysis

DSC analysis was conducted to examine the thermal properties of the zein-drug nanofibers and films prior to drug release testing. Fig. 4a represents the heat flow of the drug-zein nanofibers. As the temperature approaches 100 °C, an endothermic peak appears for each sample which indicates that bound water absorbed from air has evaporated as this point. After all the water has evaporated, heat flow steadily

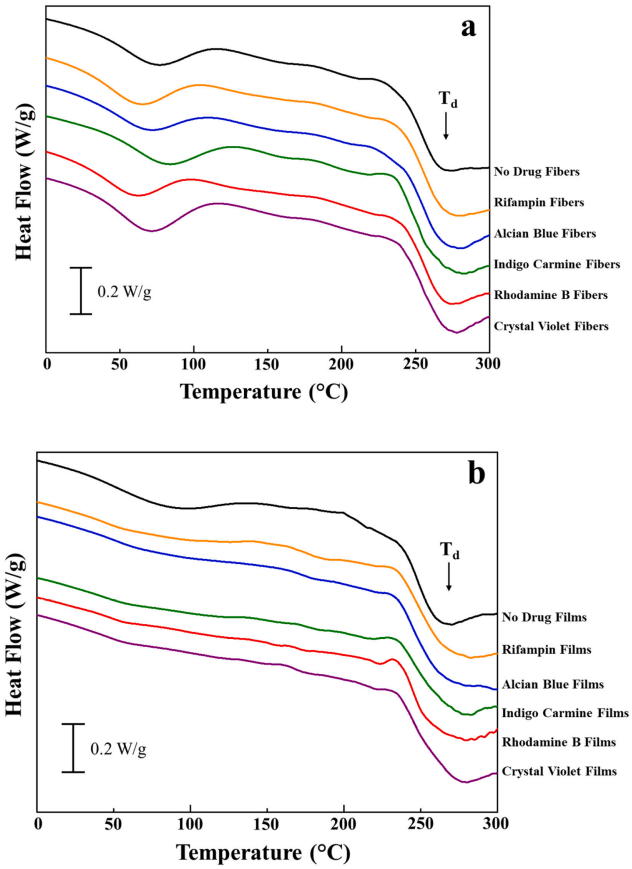

Fig. 4. Heat flow of (a) zein nanofiber and (b) zein film samples, showing temperature regions related to bound water evaporation, glass transition and degradation.

Table 2
Thermal analysis data of corn zein nanofibers and films with model drugs. Glass transition temperatures were obtained from reversing heat capacity curves, while major degradation peak temperatures were obtained from total heat flow curves (all temperature values have an error bar within ± 0.5 °C).

Sample	Fiber		Film	
	Glass transition T_g/°C	Major degradation T_d/°C	Glass transition T_g/°C	Major degradation T_d/°C
Pure corn zein	162.3	267.1	146.2	268.5
Rifampin	166.8	272.0	121.6	282.1
Alcian blue	158.2	276.9	120.1	282.9
Indigo carmine	166.2	275.6	120.4	280.9
Crystal violet	162.4	273.8	115.3	278.5
Rhodamine B	164.1	272.6	122.3	279.2

declines in each sample as temperature increases. This is due to the fact that molecules within proteins move faster in response to higher temperatures. At 226 °C, an exothermic peak occurs for corn zein nanofibers (Fig. 4a). Previous studies report that corn zein exhibits an exothermic peak at 210 °C followed by the formation of β-structures [39–41]. The higher zein exothermic peak temperature reported here is likely due to the 1-dimensional aspect of nanofibers. According to polymer nanofiber studies, nanofibers display different self-assembly behavior from those in the bulk materials [42,43]. The general trend appears to be that when model drug is present within the zein protein, the self-assembly occurs at a higher temperature. This shift is likely a result of additional molecular weight from the model drugs within the fiber mesh. This trend is consistent with every drug-zein copolymer except the alcian blue sample with an exothermic peak similar to that found in corn zein. Previously mentioned in FTIR analysis, alcian blue molecules may be too large to completely integrate into the protein structure. Corn zein polymer chains, in the alcian blue-zein copolymer, are less obstructed by the alcian blue molecules which are situated more along the polymer chain exterior rather than embedded within the alpha helical structure. Table 2 shows the full degradation peak values for each fiber sample with an average value at 273.0 ± 3.423 °C. A degradation peak appears for each fiber sample immediately after corn zein self-assembly. According to Table 2, corn zein nanofibers have a degradation peak at 267.1 °C. Previous studies have stated that corn zein powder is thermally stable up to 280 °C with a single degradation step at higher temperatures [44]. The small decrease in thermal stability is due to the increase in surface contact area where nanofiber polymer strands are exposed to more heat than in bulk material. When drugs are added to zein nanofibers, the thermal stability increases slightly and this trend is consistent throughout each sample as seen in Table 2 and Fig. 4a. However, the peak shift is minor which shows that the addition of drugs changed the molecular structure but did not significantly affect the thermal properties of the zein. This suggests that the chemical composition of the zein and the model drugs remain intact and the zein is acting solely as a carrier for the drugs. Fig. 4b represents the heat flow of the drug-zein films. The films display a similar heat flow trend seen in Fig. 4a for the nanofiber samples. Zein films have exothermic peaks immediately before degradation and display degradation in a single step. The model drug-zein films also have a major degradation peak at a higher temperature than that of the pure film, as shown in Table 2.

Fig. 5a represents the reversing heat capacity of the zein-drug nanofibers. Due to the presence of amorphous polymer, corn zein protein displays a glass transition at 162.3 °C. This is similar to the glass transition of zein powder observed in previous studies at a temperature of 165 °C [41]. As previously mentioned, the decrease in glass transition temperature is due to the polymer strands possessing more molecular mobility in the form of a nanofiber than in compact powder. In accordance with Table 2, most model drugs shift the glass transition to a

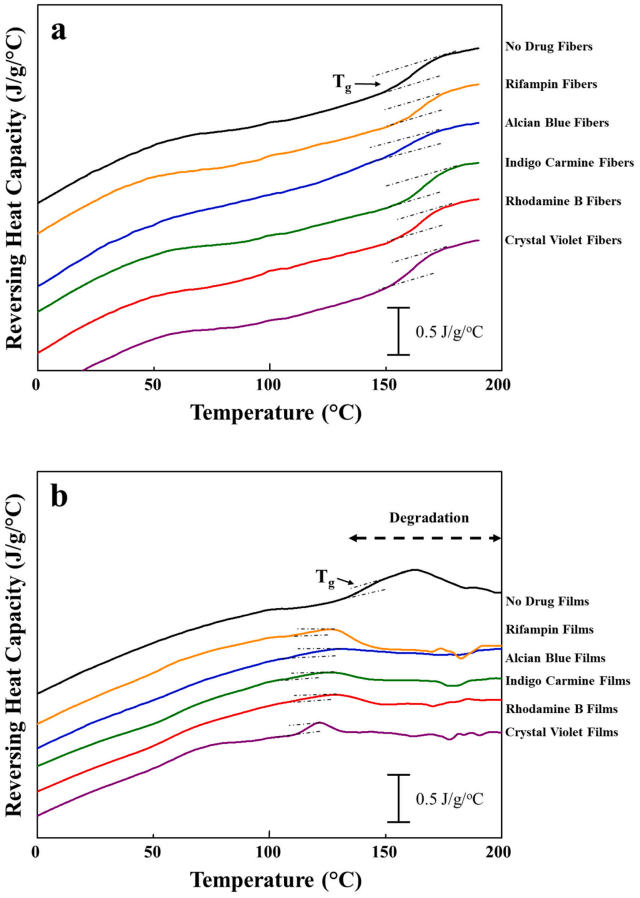

Fig. 5. Reversing heat capacity scans of different (a) zein nanofiber and (b) zein film samples, showing temperature region related glass transition temperature (T_g) vs. the reversing heat capacity for various drug-loaded samples.

higher temperature. The presence of most model drugs restricts molecular motion of the nanofiber matrix resulting in an increase in glass transition [43]. The shift in glass transition also suggests that the drugs induced molecular alignment in the zein. As described in the FTIR analysis, the drugs promote formation of alpha helical structure within the zein. Therefore, the increase in glass transition serves as evidence that there is less amorphous and more pre-aligned polymer in the drug-zein nanofibers. However, alcian blue and crystal violet samples did not follow this trend. Due to its large molecular size, alcian blue molecules push the polymer fibers together rather than embed themselves within the matrix. In addition, the melting point of alcian blue is at 148 °C which means that there was no hindrance in molecular mobility in the zein. This coincides with a decrease in glass transition in the alcian blue sample. Alcian blue likely compressed the zein polymer together into an aligned structure and melted before hindering the glass transition. In Table 2, the crystal violet-zein nanofibers exhibit a glass transition temperature value overlapping with zein protein. It appears that the crystal violet, while it induces alpha helix formation, does not impede further alignment of zein polymer.

Fig. 5b represents the reversing heat capacity of the zein-drug films with different model drugs. Zein films display an earlier glass transition than zein nanofibers which could be due to the film 2D structure having more alignment than the 1D nanofibers. Unlike the nanofibers, all films with the addition of drugs display an early glass transition (115– 123 °C, see Table 2) following with an unstable heat capacity drop, much lower than the T_g of pure zein films (146 °C). This suggested the drugs may have caused additional polymer matrix degradation or disassembling at a lower temperature (~130 °C) in the films reducing the amount of polymer available to undergo glass transition. The model

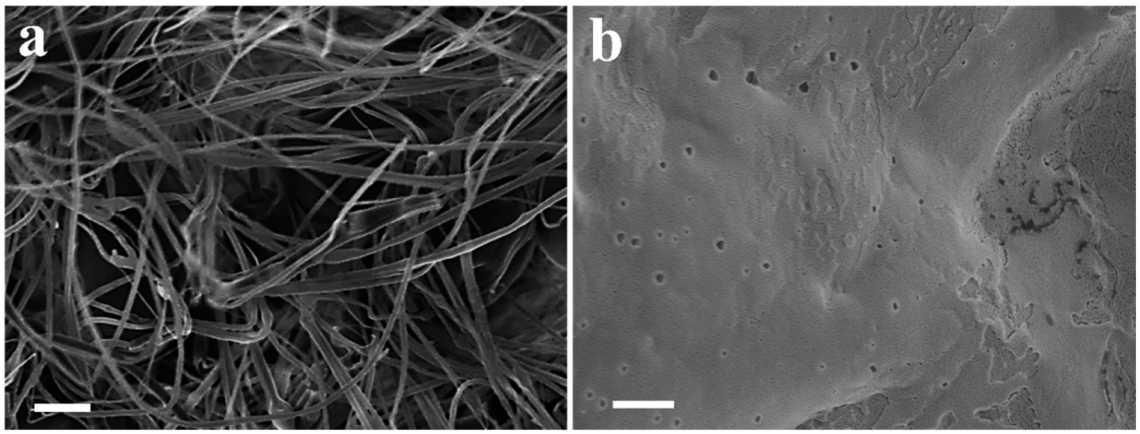

Fig. 6. SEM images of (a) pure corn zein nanofibers (scale bar is 10 μm), and the cross-section of a pure corn zein film (scale bar is 2 μm).

drugs were likely situated more along the exterior of the film unprotected inside the zein matrix. As a result, the drug release of most films is faster than that of the nanofibers because the drugs are less restricted in motion by the films (see drug release section).

3.3. Morphology characterization

The morphology and fiber diameter of the air jet spinning nanofibers are further characterized by the scanning electron microscope (SEM). As shown in Fig. 6a, the pure corn zein nanofibers are mostly uniform, with diameters at a range of 0.5 μm to 1.5 μm. The cross-section of the pure corn zein film was also characterized, showing a uniform smooth surface (Fig. 6b). No large-scale aggregates were found in the pure corn zein fiber and film samples.

SEM images of corn zein nanofibers with different model drugs are shown in Fig. 7. All five types of pre-release samples (Fig. 7, A1-E1) maintain similar morphology to the pure corn zein nanofiber, with some tiny aggregates formed randomly in the nanofiber matrix of rifampin, indigo carmine, rhodamine and crystal violet loaded fibers. The diameters of rifampin, alcian blue, indigo carmine and rhodamine samples are in the similar range compared with that of pure corn zein nanofibers. However, diameters of pre-release crystal violet nanofibers decreased to 0.2–0.8 μm. The morphology of after-release fiber samples stirring in 20 mM phosphate buffer after 7 days is shown in Fig. 7, A2-E2. Due to the release of drug into the buffer and the contraction force during the drying process, corn zein nanofibers are slowly aggregated into large particles with diameters of 0.5–1.5 μm after 7 days. Small fiber residues and holes can be found randomly on the particle surface with multi-layer structures. Both holes and layer structures could be resulted from drug release process from nanofiber matrix. While fiber samples appeared to have broken apart during release, no significant changes in mass were observed suggesting minimal degradation of zein proteins during the release.

As a comparison, the morphology of corn zein films with model drugs are shown in Fig. 8. The pre-release rifampin (A1), rhodamine (D1) and crystal violet (E1) film samples show a smooth morphology with the similar surface pattern to the pure zein film. The alcian blue (B1) film sample shows a solid and blank surface morphology. While other drug assembled into rod/particle shape and homogeneously distribute in the corn zein films. The surface of Indigo Carmine (C1) film sample tends to be rougher than other films. Due to the release of drug molecules (Fig. 8, A2-E2), holes with a similar diameter of original drug aggregates are formed on the surface of all the samples. It is worth to point out that the diameter of the holes on rifampin film surface (A2) are around 20 μm, which is much larger than that of the other four samples. The diameters of holes on the surface of alcian blue (B2) and indigo carmine (C2) samples are at a range of 1 to 4 μm, which suggest the typical size of drug aggregates in the cast films are much larger than those in the zein fibers (size of drug aggregates in fibers should be less than the average fiber diameter of 0.5–1.5 μm).

3.4. Human cell proliferation

Cell compatibility tests were performed to further demonstrate the

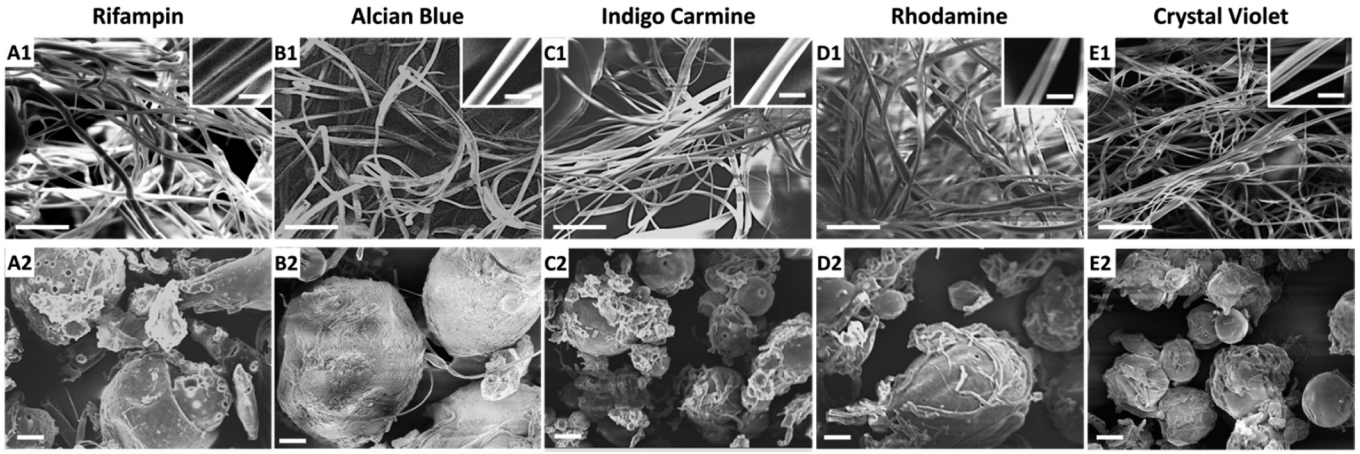

Fig. 7. SEM images of corn zein nanofibers with different model drugs. A1, B1, C1, D1 and E1 are pre-release fibers of Rifampin, Alcian Blue, Indigo Carmine, Rhodamine and Crystal Violet, respectively. The scale bar is 20 μm. The inset images are to show the diameter of individual fibers (scale bar: 2 μm). A2, B2, C2, D2 and E2 are after-release fibers of Rifampin, Alcian Blue, Indigo Carmine, Rhodamine and Crystal Violet, respectively. The scale bar is 20 μm.

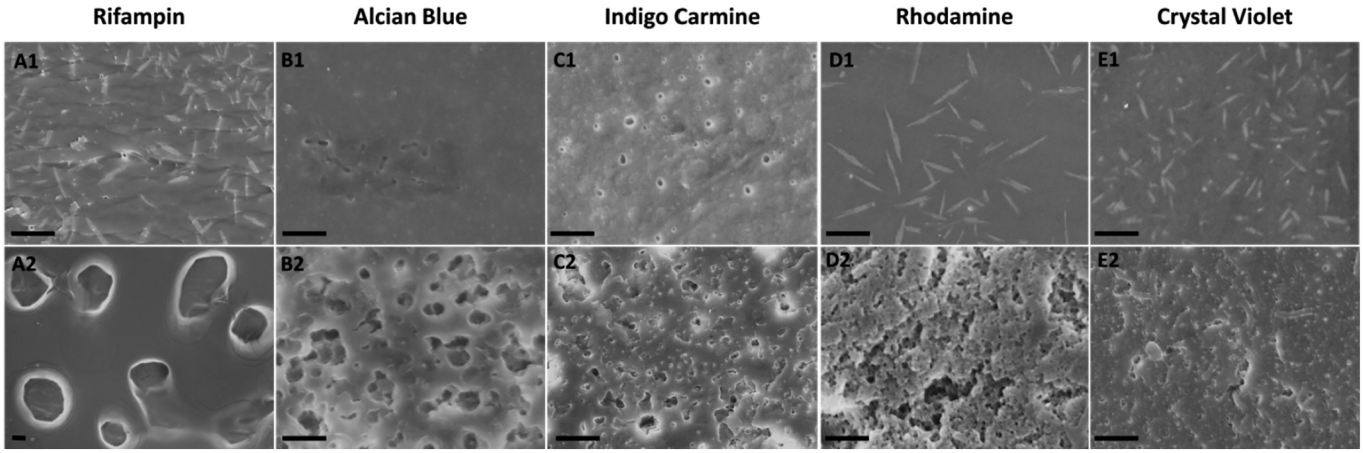

Fig. 8. SEM images of corn zein films with different model drugs. A1, B1, C1, D1 and E1 are pre-release films of Rifampin, Alcian Blue, Indigo Carmine, Rhodamine and Crystal Violet, respectively. A2, B2, C2, D2 and E2 are after-release films of Rifampin, Alcian Blue, Indigo Carmine, Rhodamine and Crystal Violet, respectively. The scale bar is 4 μm.

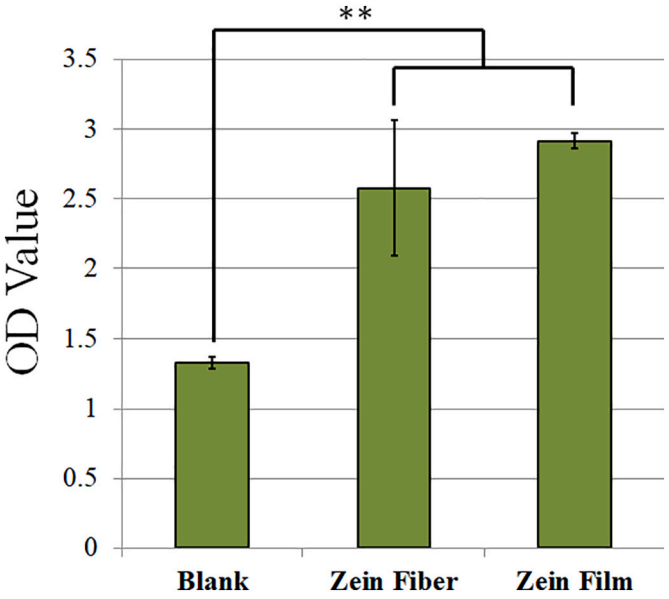

Fig. 9. HEK293 (Human embryonic kidney) cells attached to and proliferated on zein protein film and fiber materials. The cell density at 72 h was assessed using MTT assay and plotted vs. blank substrate control. The *t*-tests were performed between indicated groups (**: $p < 0.01$).

potential of zein film and nanofibers for drug release applications. HEK293 (Human embryonic kidney cells) is a cell line generated by transformation of either a fibroblastic, endothelial or epithelial cell, all of which are abundant in kidneys. These cells, if interacting with a biocompatible material in vitro, will grow and proliferate. In order to test cell compatibility on the zein materials, HEK293 cells were cultured on the surface of zein film and fiber samples (with blank substrate as the control) for 72 h. After seeding the cells on the samples for 24 and 72 h, it can be seen that the cells successfully attached to the protein fibers (24 h) and proliferated very well (72 h), similar to the cells on the films and the cells on the blank control substrates, which indicates that both zein protein materials tested in this study has good biocompatibility. Cell proliferation on both the zein fiber and film materials were then evaluated by cell numbers at 72 h after seeding using an MTT assay (Fig. 9). After 72 h, compared with blank surface, both zein film and fiber materials showed a significantly increased cell density, which indicated cell proliferation can be elevated by zein protein materials. In addition, at 72 h, the cell density on zein film samples was similar to air-spun zein fiber samples, indicating that both materials are good for biomedical applications.

3.5. Drug release study

To further investigate the potential effectiveness of the supramolecular systems for drug delivery, drug release of the model drugs incorporated in either films or fibers was simulated in 0.1% w/v 20 mM phosphate buffer (pH 7.0) for different times. These model drugs were chosen based on their similarity to existing pharmaceutical compounds, as well as varying molecular weights, hydrophobicity, and solubilities (Table 1). Some compounds such as crystal violet and rifampin, have also been shown to exhibit anti-bacterial and anti-fungal activity [45,46]. While historically used for the treatment of tuberculosis, oral delivery of rifampin was recently utilized for the treatment of atopic dermatitis [47]. Despite its therapeutic potential, oral delivery is associated with severe systemic side effects including hepatic toxicity, gastrointestinal distress, headaches, and general physical weakness [48,49]. Given their high surface area to volume ratio, porosity, and malleability, when combined with adhesive gauze, fiber mats can perform as ideal vehicles for topical drug delivery, and may be used to mitigate these side effects by allowing for localized delivery of rifampin to the skin.

Shown in Fig. 10a and b are the normalized release profiles for the fiber and film models, respectively. Data points have been normalized based on the amount of drug released at 96 h. No significant drug release was observed above 96 h for all samples. All release profiles were also fit with the Korsmeyer-Peppas model (see Eq. (1)) [36], and n values, which demonstrated the release resistance, can be shown in Table 3. In each curve fit, sufficient statistical R-squared (R^2) values suggest the validity of the model in assessing the release from both films and fiber samples. The general trends suggest that the fibers allow for sustained release. For both alcian blue and indigo carmine fiber samples, at the 15-minute time point, a considerably high release percentage is observed s. This is suggestive of a lack of bonding between the drugs and the zein protein. This further suggests that the fibers act as a physical carrier of the drugs as opposed to chemically binding to them. Alcian blue is a very large molecule (MW 1.3 kDa), so it is reasonable to assume its bulkiness prevents it from being efficiently integrated into the zein structure. In contrast to the fibers, films with indigo carmine incorporated displayed a dramatic drop at the earlier points in its release profile. This can be attributed to the nature of the method used to fabricate the films. As opposed to the fibers, due to the nature of the film synthesis, corn zein is exposed to formic acid for a longer period of time than it is during fiber generation. During this time, the formic acid

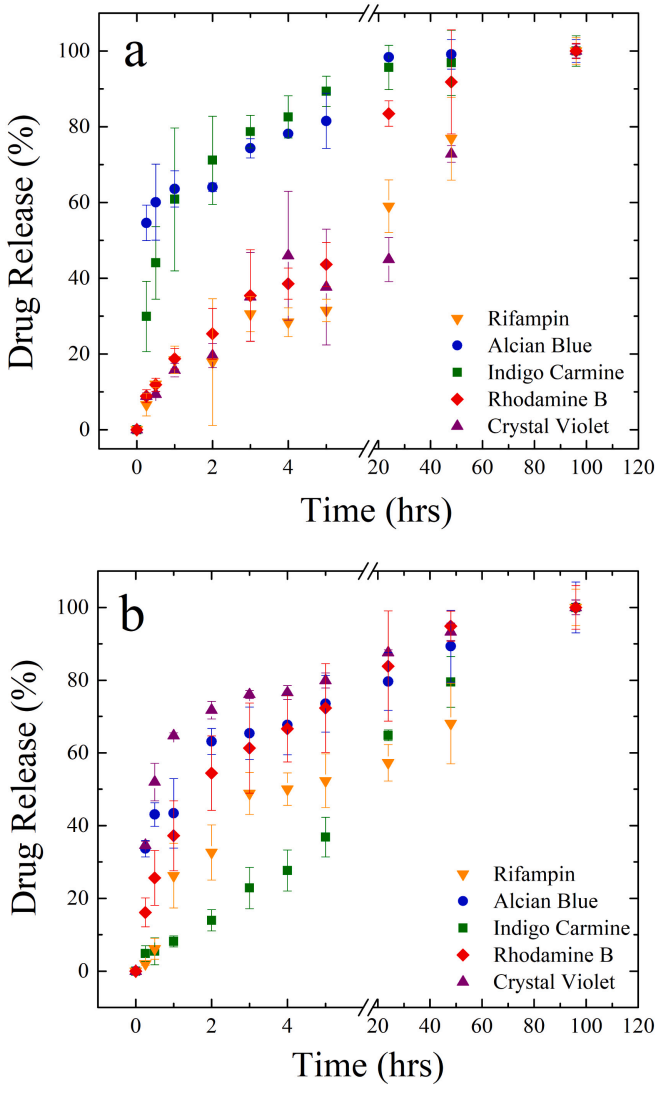

Fig. 10. Model drug release from fibers (a) and films (b). Difference between one- and two-dimensional releases can be seen. The release of most model drugs was slower and more controlled in fiber samples.

Table 3
n values from the Korsmeyer-Peppas equation of model drug release profiles from fiber and film samples shown in Fig. 10.

Model drug	Fiber		Film	
	n	R^2	n	R^2
Rifampin	0.392	0.99	0.284	0.87
Alcian blue	0.111	0.97	0.151	0.96
Indigo carmine	0.132	0.88	0.430	0.98
Crystal violet	0.353	0.93	0.118	0.93
Rhodamine B	0.337	0.95	0.203	0.91

is able to sever some of the hydrogen bonds of the corn zein structure, allowing the integration of the model drug molecules. Thus, the addition of drugs does not compress the corn zein towards a more alpha helical structure for the films allowing it to be released faster. Therefore, although the cylindrical nanofibers have a greater surface area-to-volume ratio, they are able to retain the drugs and exhibit sustained release compared to the two-dimensional films.

3.6. Mechanism of drug release

As seen in the FTIR, the addition of model drugs facilitates a transition from a network of random coils to a more alpha helical arrangement in the fiber samples. When drugs are removed, fibers revert back to their original random coil structure, showing a completely reversible, controllable transition. This is hypothesized to be caused by the binding of model drug molecules to the protein through hydrogen bonding. However, some drugs lack hydrogen bond donor groups, suggesting that their physical infiltration may facilitate the transition. It is interesting that this controllable, reversible transition is not seen in the film samples. Upon the addition of model drugs, film samples preserve their random coil structure with the exception of alcian blue, which is the largest model drug. When drug is released, in all cases film samples still consist of a network of random coils, however, there is a small shift in the FTIR, suggesting the controllable, reversible transition seen in the fibers does not take place in the films. This may be attributed to the prolonged time the films were exposed to the solvent which severed any hydrogen bonds within the proteins. A representation of this proposed mechanism of drug incorporation is shown in Fig. 11. The differing effects the model drugs have on the films and fibers can account for differences in their release profiles. It is clear that drug delivery is not solely governed by diffusion, but also the biophysical interactions between the protein and model drug molecules.

4. Conclusion

In this study, air-spun corn zein nanofibers and films were able to reversibly store a variety of model drugs. Incorporation of drug into fibers was shown to have significantly improved effect on the thermal stability of the drug molecules, while films could not prevent their thermal degradation/melting at high temperature. FTIR revealed that the original insoluble random coil network of the corn zein protein shifted to a more alpha helical structure. This change was not seen in films. Therefore, drug release from the fibers and films is not solely governed by the system geometry but rather the biophysical interaction between the corn zein protein and model drugs. This interaction was found to be dictated by the synthesis method of each system. Release from fibers was more sustained controlled in most cases, most likely due to the direct interaction between the model drugs and protein. Understanding this interaction in more detail can lead to more efficient design of protein-based drug delivery systems.

CRediT authorship contribution statement

Kelsey DeFrates: Formal analysis, Validation, Investigation, Writing - original draft, Visualization. **Theodore Markiewicz**: Formal analysis, Validation, Investigation, Writing - original draft, Visualization. **Ye Xue**: Investigation, Data curation, Formal analysis. **Kayla Callaway**: Investigation, Data curation, Formal analysis. **Christopher Gough**: Investigation, Data curation. **Robert Moore**: Investigation, Data curation. **Kristen Bessette**: Investigation, Data curation. **Xiaoyang Mou**: Conceptualization, Investigation, Data curation, Formal analysis. **Xiao Hu**: Conceptualization, Methodology, Validation, Supervision, Project administration, Formal analysis, Funding acquisition, Writing - review & editing, Resources.

Declaration of competing interest

The authors declare that they have no known competing financial interests or personal relationships that could have appeared to influence the work reported in this paper.

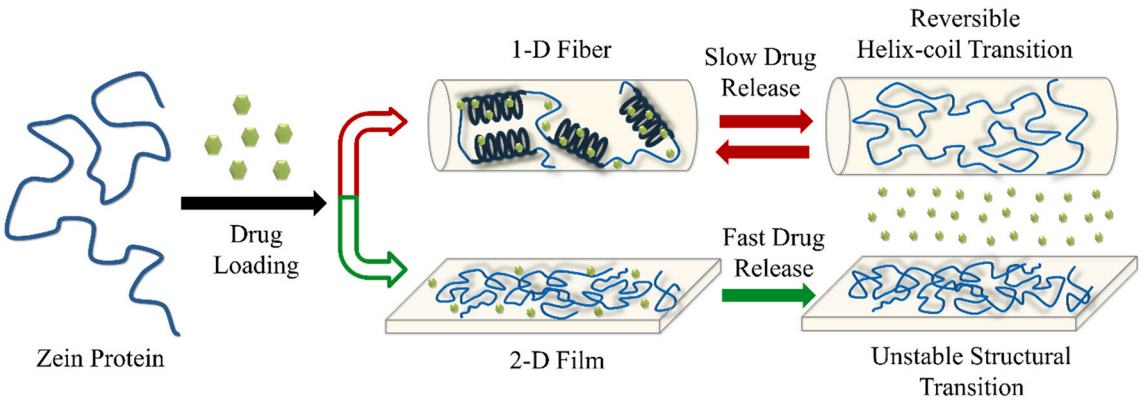

Fig. 11. Proposed mechanism for the loading and release of drugs from corn zein nanofibers and films. In air-spun fiber samples, the addition of drugs causes the random coil network to transition to a more alpha helical structure. Once drugs are removed, samples return to their native structure. In films, the addition of drugs does not cause the formation of alpha helices, but the original random coil network is not conserved.

Acknowledgment

This study was supported by the Rowan University Start-up Grants. X.H. is also supported by the US NSF Biomaterials Program (DMR-1809541). The authors would also like to thank Dave Jao for his suggestions on this study.

Appendix A. Supplementary data

Supplementary data to this article can be found online at https://doi.org/10.1016/j.msec.2020.111419.

References

[1] R. Goyal, L.K. Macri, H.M. Kaplan, J. Kohn, Nanoparticles and nanofibers for topical drug delivery, J. Control. Release 240 (2016) 77–92.
[2] W. Cui, Y. Zhou, J. Chang, Electrospun nanofibrous materials for tissue engineering and drug delivery, Sci. Technol. Adv. Mater. 11 (1) (2010) 014108.
[3] C.C. Müller-Goymann, Physicochemical characterization of colloidal drug delivery systems such as reverse micelles, vesicles, liquid crystals and nanoparticles for topical administration, Eur. J. Pharm. Biopharm. 58 (2) (2004) 343–356.
[4] D. Šmejkalová, T. Muthný, K. Nešporová, M. Hermannová, E. Achbergerová, G. Huerta-Angeles, M. Svoboda, M. Čepa, V. Machalová, D. Luptáková, V. Velebný, Hyaluronan polymeric micelles for topical drug delivery, Carbohydr. Polym. 156 (2017) 86–96.
[5] S. Gungor, M. Rezigue, Nanocarriers mediated topical drug delivery for psoriasis treatment, Curr. Drug Metab. 18 (5) (2017) 454–468.
[6] H.A.E. Benson, Elastic liposomes for topical and transdermal drug delivery, in: G.G.M. D'Souza (Ed.), Liposomes: Methods and Protocols, Springer New York, New York, NY, 2017, pp. 107–117.
[7] Y. Goh, I. Shakir, R. Hussain, Electrospun fibers for tissue engineering, drug delivery, and wound dressing, J. Mater. Sci. 48 (2013) 3027–3054.
[8] R. Langasco, B. Cadeddu, M. Formato, A.J. Lepedda, M. Cossu, P. Giunchedi, R. Pronzato, G. Rassu, R. Manconi, E. Gavini, Natural collagenic skeleton of marine sponges in pharmaceutics: innovative biomaterial for topical drug delivery, Mater. Sci. Eng. C 70 (2017) 710–720.
[9] D. Chantasart, P. Tocanitchart, A. Wongrakpanich, V. Teeranachaideekul, V.B. Junyaprasert, Fabrication and evaluation of Eudragit® polymeric films for transdermal delivery of piroxicam, Pharm. Dev. Technol. 23 (8) (2018) 771–779.
[10] K. Saha, B.S. Butola, M. Joshi, Drug-loaded polyurethane/clay nanocomposite nanofibers for topical drug-delivery application, J. Appl. Polym. Sci. 131 (10) (2014) 40230.
[11] R. Vasita, D.S. Katti, Nanofibers and their applications in tissue engineering, Int. J. Nanomedicine 1 (1) (2006) 15–30.
[12] D. Li, Y. Xia, Electrospinning of nanofibers: reinventing the wheel? Adv. Mater. 16 (14) (2004) 1151–1170.
[13] J. Yang, K. Wang, D.-G. Yu, Y. Yang, S.W.A. Bligh, G.R. Williams, Electrospun Janus nanofibers loaded with a drug and inorganic nanoparticles as an effective antibacterial wound dressing, Mater. Sci. Eng. C 111 (2020) 110805.
[14] K. Wang, P. Wang, M. Wang, D. Yu, W. Fuxian, A. Bligh, Comparative study of electrospun crystal-based and composite-based drug nano depots, Mater. Sci. Eng. C 110988 (2020).
[15] S. Chang, M. Wang, F. Zhang, Y. Liu, X. Liu, D.-G. Yu, H. Shen, Sheath-separate-core nanocomposites fabricated using a trifluid electrospinning, Mater. Des. 192 (2020) 108782.
[16] M. Wang, K. Wang, Y. Yang, Y. Liu, D.G. Yu, Electrospun environment remediation nanofibers using unspinnable liquids as the sheath fluids: a review, Polymers 12 (1) (2020) 103.
[17] X. Shi, W. Zhou, D. Ma, Q. Ma, D. Bridges, Y. Ma, A. Hu, Electrospinning of nanofibers and their applications for energy devices, J. Nanomater. 2015 (2015) 140716.
[18] S. Sinha-Ray, S. Sinha-Ray, A.L. Yarin, B. Pourdeyhimi, Theoretical and experimental investigation of physical mechanisms responsible for polymer nanofiber formation in solution blowing, Polymer 56 (2015) 452–463.
[19] E. Stojanovska, E. Canbay, E.S. Pampal, M.D. Calisir, O. Agma, Y. Polat, R. Simsek, N.A.S. Gundogdu, Y. Akgul, A. Kilic, A review on non-electro nanofibre spinning techniques, RSC Adv. 6 (87) (2016) 83783–83801.
[20] A. Abdal-hay, A.S. Hamdy, J.H. Lim, Facile preparation of titanium dioxide micro/nanofibers and tubular structures by air jet spinning, Ceram. Int. 40 (10) (2014) 15403–15409.
[21] Y. Li, L.T. Lim, Y. Kakuda, Electrospun Zein fibers as carriers to stabilize (−)-Epigallocatechin Gallate, J. Food Sci. 74 (3) (2009) C233–C240.
[22] M. Wang, T. Hai, Z. Feng, D.-G. Yu, Y. Yang, S.A. Bligh, The relationships between the working fluids, process characteristics and products from the modified coaxial electrospinning of zein, Polymers 11 (8) (2019) 1287.
[23] X. Liu, Q. Sun, H. Wang, L. Zhang, J.-Y. Wang, Microspheres of corn protein, zein, for an ivermectin drug delivery system, Biomaterials 26 (1) (2005) 109–115.
[24] J. Dong, Q. Sun, J.-Y. Wang, Basic study of corn protein, zein, as a biomaterial in tissue engineering, surface morphology and biocompatibility, Biomaterials 25 (19) (2004) 4691–4697.
[25] C. Kimna, S. Tamburaci, F. Tihminlioglu, Novel zein-based multilayer wound dressing membranes with controlled release of gentamicin, J. Biomed. Mater. Res. B Appl. Biomater. 107 (6) (2019) 2057–2070.
[26] Y. Wang, M. Zhao, S.A. Barker, P. Belton, D. Craig, A spectroscopic and thermal investigation into the relationship between composition, secondary structure and physical characteristics of electrospun zein nanofibers, Mater. Sci. Eng. C 98 (2019) 409–418.
[27] H. Lu, Y. Qiu, Q. Wang, G. Li, Q. Wei, Nanocomposites prepared by electrohydrodynamics and their drug release properties, Mater. Sci. Eng. C 91 (2018) 26–35.
[28] W. Huang, T. Zou, S. Li, J. Jing, X. Xia, X. Liu, Drug-loaded Zein Nanofibers prepared using a modified coaxial electrospinning process, AAPS PharmSciTech 14 (2) (2013) 675–681.
[29] Y. Wang, G.W. Padua, Nanoscale characterization of zein self-assembly, Langmuir: the ACS Journal of Surfaces and Colloids 28 (5) (2012) 2429–2435.
[30] D. Jao, Y. Xue, J. Medina, X. Hu, Protein-based drug-delivery materials, Materials 10 (5) (2017) 517.
[31] T.J. Anderson, B.P. Lamsal, REVIEW: zein extraction from corn, Corn Products, and Coproducts and Modifications for Various Applications: A Review, Cereal Chemistry Journal 88 (2) (2011) 159–173.
[32] E.A. Simone, T.D. Dziubla, V.R. Muzykantov, Polymeric carriers: role of geometry in drug delivery, Expert Opinion on Drug Delivery 5 (12) (2008) 1283–1300.
[33] E.-R. Kenawy, F.I. Abdel-Hay, M.H. El-Newehy, G.E. Wnek, Processing of polymer nanofibers through electrospinning as drug delivery systems, Mater. Chem. Phys. 113 (1) (2009) 296–302.
[34] S. Tungprapa, I. Jangchud, P. Supaphol, Release characteristics of four model drugs from drug-loaded electrospun cellulose acetate fiber mats, Polymer 48 (17) (2007) 5030–5041.
[35] Y. Li, J. Li, Q. Xia, B. Zhang, Q. Wang, Q. Huang, Understanding the dissolution of α-zein in aqueous ethanol and acetic acid solutions, J. Phys. Chem. B 116 (39) (2012) 12057–12064.
[36] P. Costa, J.M. Sousa Lobo, Modeling and comparison of dissolution profiles, Eur. J. Pharm. Sci. 13 (2) (2001) 123–133.
[37] A.M. Díez-Pascual, A.L. Díez-Vicente, Development of linseed oil-TiO2 green nanocomposites as antimicrobial coatings, J. Mater. Chem. B 3 (21) (2015) 4458–4471.
[38] K. DeFrates, T. Markiewicz, K. Callaway, Y. Xue, J. Stanton, D. Salas-de la Cruz, X. Hu, Structure–property relationships of Thai silk–microcrystalline cellulose

biocomposite materials fabricated from ionic liquid, Int. J. Biol. Macromol. 104 (2017) 919–928.
[39] J. Magoshi, S. Nakamura, K.-I. Murakami, Structure and physical properties of seed proteins. I. Glass transition and crystallization of zein protein from corn, Journal of Applied Polymer Science 45(11) (1992) 2043-2048.
[40] R. Shukla, M. Cheryan, Zein: the industrial protein from corn, Ind. Crop. Prod. 13 (3) (2001) 171–192.
[41] J. Magoshi, S. Nakamura, BIODEGRADABLE POLYMER IN SEED PROTEIN FROM CORN A2 - KENNEDY, JOHN F, in: G.O. Phillips, P.A. Williams (Eds.), Recent Advances in Environmentally Compatible Polymers, Woodhead Publishing2001, pp. 247–257.
[42] P. Samanta, R. Srivastava, B. Nandan, H.-L. Chen, Crystallization behavior of crystalline/crystalline polymer blends under confinement in electrospun nanofibers of polystyrene/poly(ethylene oxide)/poly(ε-caprolactone) ternary mixtures, Soft Matter 13 (8) (2017) 1569–1582.
[43] F. Navarro-Pardo, G. Martínez-Barrera, A. Martínez-Hernández, V. Castaño, J. Rivera-Armenta, F. Medellín-Rodríguez, C. Velasco-Santos, Effects on the thermo-mechanical and crystallinity properties of nylon 6,6 electrospun fibres reinforced with one dimensional (1D) and two dimensional (2D) carbon, Materials 6 (8) (2013) 3494.
[44] E. Corradini, P. Curti, A. Meniqueti, A. Martins, A. Rubira, E. Muniz, Recent advances in food-packing, pharmaceutical and biomedical applications of zein and zein-based materials, Int. J. Mol. Sci. 15 (12) (2014) 22438.
[45] A.M. Maley, J.L. Arbiser, Gentian violet: a 19th century drug re-emerges in the 21st century, Exp. Dermatol. 22 (12) (2013) 775–780.
[46] A.M. Loeffler, Uses of rifampin for infections other than tuberculosis, Pediatr. Infect. Dis. J. 18 (7) (1999) 631–632.
[47] S.H. Kim, K.M. Lee, G.S. Lee, J.W. Seong, T.J. Kang, Rifampicin alleviates atopic dermatitis-like response in vivo and in vitro, Biomol. Ther. 25 (6) (2017) 634–640.
[48] J.S. Patil, V.K. Devi, K. Devi, S. Sarasija, A novel approach for lung delivery of rifampicin-loaded liposomes in dry powder form for the treatment of tuberculosis, Lung India: official organ of Indian Chest Society 32 (4) (2015) 331–338.
[49] A.K. Dutt, D. Moers, W.W. Stead, Undesirable side effects of isoniazid and rifampin in largely twice-weekly short-course chemotherapy for tuberculosis, Am. Rev. Respir. Dis. 128 (3) (1983) 419–424.